J Sol-Gel Sci Technol (2013) 66:238–241
DOI 10.1007/s10971-013-2999-4

ORIGINAL PAPER

Preparation of $BaFe_{12}O_{19}$ as anode material for lithium-ion batteries through sol–gel method

Yang Zhao · Ying Huang · Qiufen Wang · Yan Wang · Meng Zong

Received: 8 January 2013 / Accepted: 28 February 2013 / Published online: 7 March 2013

Abstract The $BaFe_{12}O_{19}$ nanocrystalline was prepared via a sol–gel process. The structure, morphology and electrochemical properties of the nanocrystallines were detected by means of XRD, TEM, TGA and electrochemical measurements. This $BaFe_{12}O_{19}$ is firstly used as anode electrode material for lithium-ion batteries. The mechanism of $BaFe_{12}O_{19}$ with Li will also be discussed. The reversible specific capacity of $BaFe_{12}O_{19}$ is 959.5 mAh/g. A capacity of 358.3 mAh/g can be retained after 50 cycles which will have a broad space for improvement with modifying.

Keywords Ferrite-$BaFe_{12}O_{19}$ · Sol–gel method · Energy storage and conversion · Electrochemical properties · Anode material

1 Introduction

The lithium-ion battery is considered to be an excellent portable electronic products and electric vehicle power. At present, the carbon materials have been commercialized, but it has a relatively low theoretical capacity (372 mAh/g) [1, 2]. The transition metal oxides [3–5] have received increasing attention due to their high capabilities, especially the iron oxides [6, 7]. A variety of morphologies of the Fe_2O_3 and Fe_3O_4 have been prepared [8–10]. The ferrite, as a type of magnetic material, has already been intensively researched [11, 12]. This material has attracted for its application in the magnetic property. However, as the complex iron oxides [13], the ferrites could also be intercalated/deintercalated with lithium-ion in theoretically. The ferrite anodes, like $NiFe_2O_4$ [14], $ZnFe_2O_4$ [15], $CoFe_2O_4$ [16], and $CaFe_2O_4$ [17], have gained in significance due to their high specific capacities. The initial charge capacities of these ferrite materials usually exceed 900 mAh/g, which are much higher than the commonly used carbon materials. The use of transition-metal nanoparticles to enhance surface electrochemical reactivity will lead to further improvements in the performance of lithium-ion batteries [18]. The ferrites have become the potential anode materials for lithium-ion batteries.

However, the researches of the ferrites, as the anode materials, are still concentrated on the simple iron-transition metal oxides: MFe_2O_4 [19]. To our knowledge, there have been no reports in the electrochemical behavior on nanocrystalline $BaFe_{12}O_{19}$. In the first time, we try to use this complex ferrite-$BaFe_{12}O_{19}$ as anode material for lithium-ion batteries and study its Li-storage mechanism. Through our research, the type of the anode electrode materials will be expanded.

2 Experimental

The $BaFe_{12}O_{19}$ nanocrystalline ferrite was prepared by a sol–gel process [11]. Firstly, citric acid was dissolved in deionized water. Then $Fe(NO_3)_3 9H_2O$, $Ba(NO_3)_2$ were added into the citric acid solution and stirred under room temperature. The PH of the solution was adjusted to 7 by adding glycol and quadrol. The mixed solution was evaporated in a blender at 75 °C to remove surplus water until a

Y. Zhao · Y. Huang (✉) · Q. Wang · Y. Wang · M. Zong
The Key Laboratory of Space Applied Physics and Chemistry, Ministry of Education, Department of Applied Chemistry, School of Science, Northwestern Polytechnical University, Xi'an 710072, People's Republic of China
e-mail: yingh@nwpu.edu.cn

Y. Zhao
e-mail: zhaoyang890@163.com

viscous liquid was obtained. The gel was then dried at 120 °C about 24 h. Subsequently, the dried gel was pre-sintered for 5 h at 400 °C.Finally, the gel was calcined at 800 °C for 2 h to form the nanocrystalline.

The structures of the prepared samples were characterized by X-ray diffraction analysis (XRD) (Rigaku, model D/max-2500 system at 40 kV and 100 mA of Cu Kα). The surface morphology of the nanocrystallines were performed by model Tecnai F30 G2 (FEI CO., USA) field emission transmission electron microscope (FETEM).

Electrochemical performance was evaluated by a CR2016-type coin cell with a multi-channel current static system Land (LAND CT200IA). The anode electrodes were prepared by coating slurries consisting of $BaFe_{12}O_{19}$ nanocrystalline (60 wt%) with acetylene black (20 wt%) and PVDF (20 wt%) as a binder dissolved in 1-methyl-2-pyrrolidinone(NMP) solution on a copper foil. Li foil was used as counter electrode, polypropylene (PP) film (Celgard 2400) as separator. The electrolyte was a solution of 1 M $LiPF_6$ in a mixture of ethylene (EC), dimethyl carbonate (DMC) and diethyl carbonate (DEC) (1:1:1, v/v/v). Cyclic voltammetry (CV) was performed on a Series G 750^{TM} Redefining Electrochemical Measurement (USA GMARY Co.).

3 Results and discussion

3.1 Characterization of the as-prepared $BaFe_{12}O_{19}$

The XRD pattern of the as-prepared $BaFe_{12}O_{19}$ is shown in Fig 1a. The calculated lattice parameters are a = 5.892 Å, b = 5.892 Å, c = 23.198 Å. All strong diffraction lines can be indexed to the standard $BaFe_{12}O_{19}$ phase (PDF = #39-1433), indicating the strong crystalline nature of the $BaFe_{12}O_{19}$. Figure 1b shows the TGA curve of the $BaFe_{12}O_{19}$.There is a weak weight loss before 200 °C, which is due to the evaporation of absorbed water. The weight loss from 200 to 400 °C can be contributed to the decomposition of citric acid and organic combustion. And in around 800 °C, the crystal transformation happens. Figure 1c shows the TEM image of the as prepared $BaFe_{12}O_{19}$ nanocrystallines. The crystallite sizes of the $BaFe_{12}O_{19}$ are about 50–100 nm. The sizes of the sample particles are relatively uniform.

3.2 Discussion on mechanism

According to the report [20], the reaction mechanism of ferrites with Li is different from classical Li insertion/extraction process.

Figure 2a shows the CV curves of the first, second and fifth cycles of $BaFe_{12}O_{19}$. In the first cycle, a spiky peak appears at about 0.5 V and a large wide peak exists at about

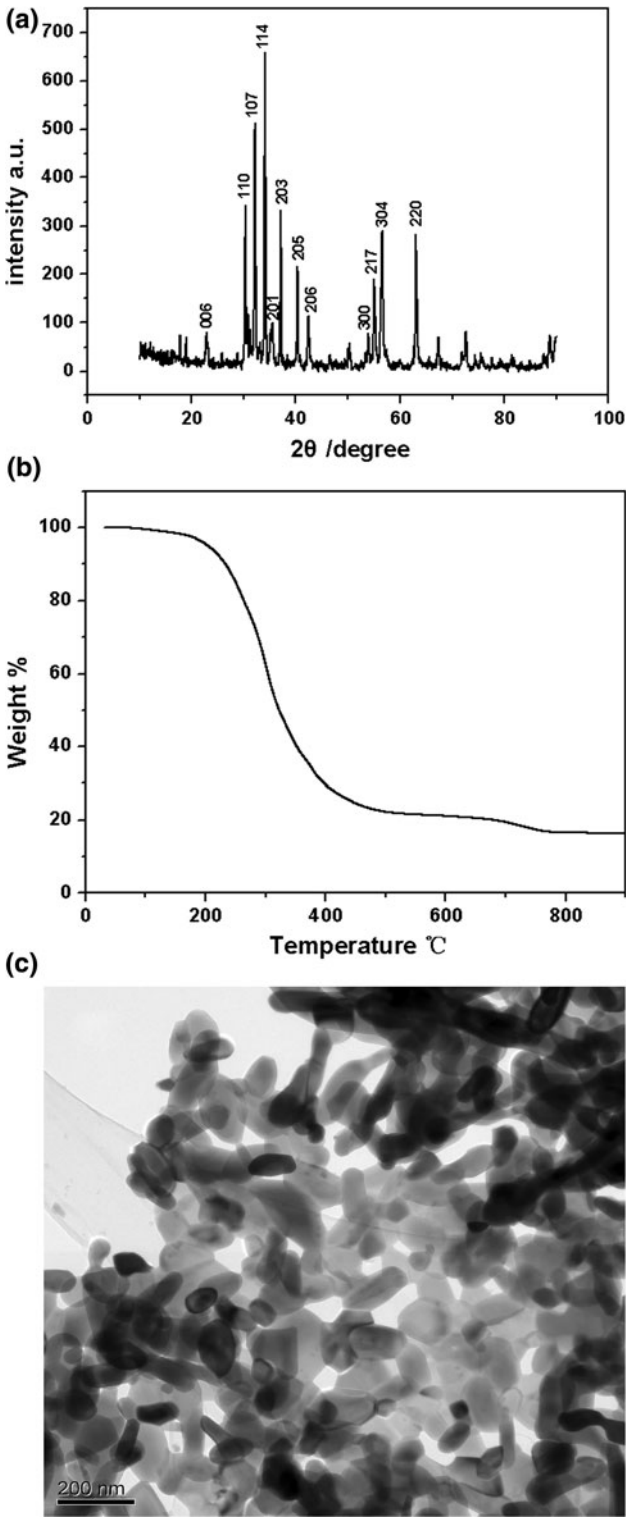

Fig. 1 The XRD pattern (**a**) the TGA curve (**b**) and the TEM images (**c**) of the as-prepared $BaFe_{12}O_{19}$

1.25 V. In the next cycle, the peak at about 0.5 V moves slightly to 0.6 V. The spiky reduction peak at about 0.5 V can be attributed to the reduction of Ba(II) and Fe(III) to their metallic states. For the second and fifth cycles, the

peak at 0.6 V is relative to the reversible reduction reaction of Fe_2O_3 and BaO. The anodic peak at 2 V can be attributed to the oxidation of the metallic iron and barium into Fe(III) and Ba(II).

For a further understanding of the first discharge process, the structures of the intermediate states of the electrodes while discharged to 1.0 and 0.3 V are examined by XRD analyses. Figure 2b shows the XRD pattern. H1 in Fig. 2b shows the original $BaFe_{12}O_{19}$ electrode before cycling. H2 and H3 show the $BaFe_{12}O_{19}$ electrodes which discharge to 1 V and 0.3 V, respectively. During the first discharge process, the $BaFe_{12}O_{19}$ gradually decreases with the voltage reduction. In the end of the reaction, the $BaFe_{12}O_{19}$ changes into Fe, Ba and the $BaFe_{12}O_{19}$ nanocrystalline thoroughly decomposes. So, the Li storage mechanism of $BaFe_{12}O_{19}$ is proposed as follows [15, 21]:

$$BaFe_{12}O_{19} + 38Li^+ + 38e^- \rightarrow 19Li_2O + 12Fe + Ba \quad (1)$$

$$Ba + Li^+ + e^- \rightarrow LiBa\ (alloy) \quad (2)$$

.

In the following recharge process, the ferrite molecule cannot be recovered and the reactions proceed as follows [18]:

$$Li_2O + Fe \leftrightarrow 6Li^+ + Fe_2O_3 + 6e^- \quad (3)$$

$$Li_2O + Ba \leftrightarrow BaO + 2Li^+ + 2e^- \quad (4)$$

$$LiBa(alloy) \rightarrow Li^+ + Ba + e^- \quad (5)$$

.

Based on the above-mentioned mechanisms, the discharge in the first cycle is essentially the destruction of the crystal structure. The formation of Li_2O is partially irreversible and contributes to the irreversible capacity loss in the first cycle. Additionally, the formation of the solid electrolyte interphase (SEI) film layer is also partially responsible for the initial irreversible capacity loss [15]. As usual, Li_2O is identified to be electrochemically inactive, but in the case of nano-sized metal particles, the electrochemical activity towards the formation/decomposition of Li_2O can be improved [22].Hence, in the following cycles, both Li–Ba alloy and three-phase region between metal oxides, Fe(Ba) and Li_2O provide reversible electrochemical reaction toward Li.

3.3 Electrochemical performance

Figure 3a presents the discharge–charge curves of the $BaFe_{12}O_{19}$ electrode in the voltage range of 0.01–2.0 V at a current density of 0.1 C. The first discharge starts from the open circuit voltage and the working voltage falls rapidly to 1 V. Within the 1.0–0.6 V range, the voltage maintains a long plateau that is followed by a sloping curve to the cut-off voltage of 0.01 V. The first-charge curve shows a smooth increasing profile with a plateau voltage at 1.5 V. [15]. In the first cycle, the $BaFe_{12}O_{19}$ delivers a lithium insertion capacity of 1,538 mAh/g and a reversible charging capacity of 959.5 mAh/g. The irreversible discharge capacity after the first cycle is unlikely/unexpectedly gone away due to severe side reaction with the electrolyte to form Li_2O and SEI film [23]. The galvanostatic charge/discharge cycling results are shown in Fig. 3b. The reversible specific capacity of $BaFe_{12}O_{19}$ is 959.5 mAh/g. The capacity has attenuated to 358.3 mAh/g at the 50th cycle. Thus the irreversible capacity loss between the first discharge and the charge cycle is 62.3 %, which matches with the mechanism discussed above. Beginning with the second cycle, the coulombic efficiency has been stabilized and approaches 99 % at the 50th cycle.

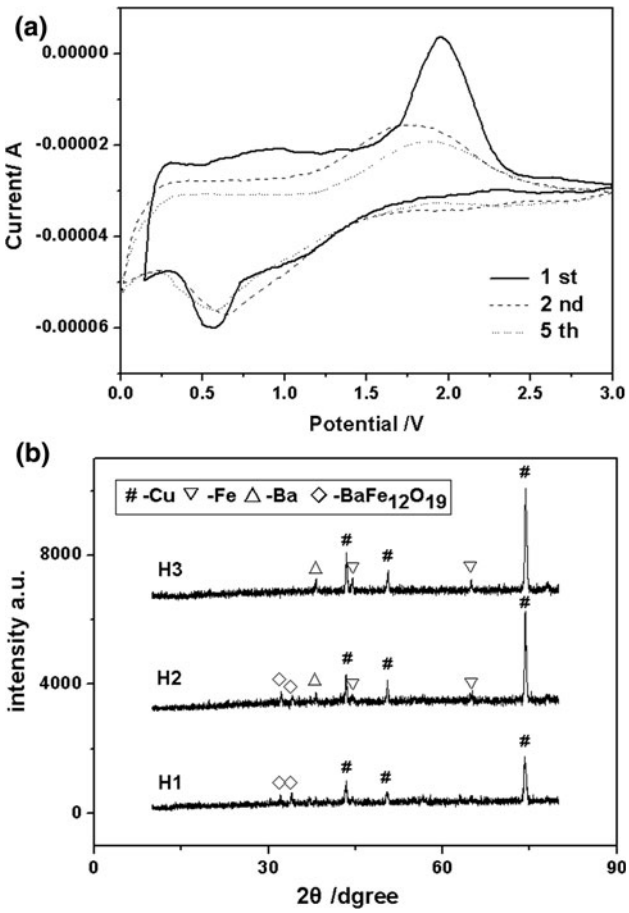

Fig. 2 The CV curves of the first, second and fifth cycles of $BaFe_{12}O_{19}$ (**a**) : The XRD patterns of the $BaFe_{12}O_{19}$ electrode (**b**): (H1) original $BaFe_{12}O_{19}$ electrode, (H2) discharge to 1 V in the initial cycle, (H3) discharge to 0.3 V in the first cycle

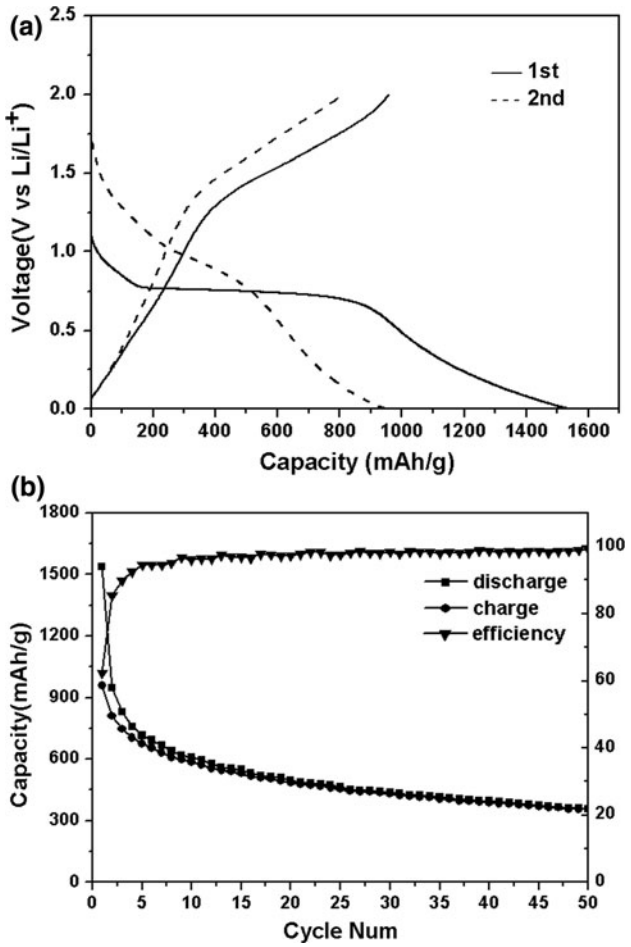

Fig. 3 The first two discharge–charge curves of the $BaFe_{12}O_{19}$ electrode (**a**): Plot of capacity; coulombic efficiency versus cycle number for $BaFe_{12}O_{19}$ (**b**)

4 Conclusions

In summary, a nanocrystalline $BaFe_{12}O_{19}$ was synthesized via sol–gel process under mild conditions. This is the first time that the $BaFe_{12}O_{19}$ is used as anode electrode material for lithium-ion batteries. The mechanism of $BaFe_{12}O_{19}$ with Li^+ is different from classical Li insertion and extraction or Li alloying process. The reversible specific capacity of $BaFe_{12}O_{19}$ is 959.5 mAh/g. A capacity of 358.3 mAh/g can be retained after 50 cycles.

Acknowledgments This work was supported by the Spaceflight Foundation of the People's Republic of China under Grant no. N8XW0002. This work was supported by the Graduate Starting Seed Fund of Northwestern Polytechnical University no. Z2013146.

References

1. Zhao Y, Huang Y, Wang QF, Wang XY, Zong M (2013) Ceram Int 39:1741–1747
2. Wang QF, Huang Y, Miao J, Zhao Y, Wang Y (2012) Mater Lett 71:66–69
3. Guo BK, Chi MF, Suna XG, Dai S (2012) J Power Sources 205:495–499
4. Lu Y, Wang Y, Zou YQ, Jiao Z, Zhao B, He YQ (2010) Electrochem Commun 12:101–105
5. Wang F, Tao WZ, Zhao MS, Xu MW, Yang SC, Sun ZB, Wang LQ, Song XQ (2011) J Alloy Compd 509:798–803
6. Hassan MF, Guo ZP, Chen ZX, Liu HK (2011) Mater Res Bull 46:858–864
7. Chen YX, He LH, Shang PJ, Tang QL, Liu ZQ, Liu HB (2011) J Mater Sci Technol 27:41–45
8. Shi C, Cao T, Cao CB, Wu DJ, Li YN, Wang MN, Mo W (2012) Mater Lett 83:35–38
9. Zhang JJ, Yao Y, Huang T, Yu A (2012) Electrochim Acta 78:502–507
10. Chen JS, Zhang YM, Lou XW (2011) ACS Appl Mater Interfaces 3:3276–3279
11. Wang Y, Huang Y, Wang QF (2012) J Magn Magn Mater 324:3024–3028
12. Wu YF, Huang Y, Niu L, Zhang YL, Li YQ, Wang XY (2012) J Magn Magn Mater 324:616–621
13. Xu Y, Li YJ, Liu SQ, Li HL, Liu YN (2012) J Power Sources 220:103–107
14. Li XD, Yang WS, Li F, Evans DG, Duan X (2006) J Phys Chem Solids 607:1286–1290
15. Ding Y, Yang YF, Shao HX (2011) Electrochim Acta 56:9433–9438
16. Xia H, Zhu DD, Fu YS, Wang X (2012) Electrochim Acta 83:166–174
17. Sharma N, Shaju KM, Subba Rao GV, Chowdari BVR (2003) J Power Sources 124:204–212
18. Sivakumar N, Gnanakan SRP, Karthikeyan K, Amaresh S, Yoon WS, Park GJ, Lee YS (2011) J Alloy Compd 509:7038–7041
19. Ding Y, Yang YF, Shao HX (2012) Solid State Ionics 217:27–33
20. Goodenough JB, Kim Y (2010) Chem Mater 22:587–603
21. Guo XW, Lu X, Fang XP, Mao Y, Wang ZX, Chen LQ (2010) Electrochem Commun 12:847–850
22. Wang GX, Chen Y, Konstantinov Y, Lindsay M, Liu HK, Dou SX (2002) J Power Sources 109:142–147
23. Wang QF, Huang Y, Miao J, Zhao Y, Wang Y (2012) Appl Surf Sci 258:6923–6929